scientific reports

Check for updates

OPEN

Self-assembled sub-picoliter liquid periodic structures in a hollow optical fiber

Sohee An[1,2], Sunghoon Jeong[1], Jihyun Hwang[1,3], Yongmin Jung[4], Jongki Kim[1,5] & Kyunghwan Oh[1]✉

In an experimental exploration, we successfully implemented a self-assembling methodology to construct a periodic liquid-air structure inside a hollow optical fiber (HOF). This fiber comprises a central air hole, a germanosilica ring core, and a silica cladding. A periodic structure of liquid droplets and air was obtained by the application of a microscopic heat source (MHS) traversing along the axial direction of the liquid-filled HOF. In the course of this study, we discerned three distinct zones within the structure. The first zone, referred to as Zone 1, demonstrated near-constant periodicity. The second zone, Zone 2, exhibited adaptable properties with regard to its periodicity, allowing it to be flexibly controlled. In the third zone, Zone 3, we noticed a chaotic response to external parameters, including temperature and the speed at which MHS was traversed. To regulate the liquid-air periodic structures, two different types of MHSs were utilized - a micro hydro-oxygen torch and a metal ring heater, each mounted on a translation stage. The study provides a detailed account of the parameters employed in utilizing these MHSs. Additionally, the optical properties of these liquid-air periodic structures were meticulously analyzed to explore the potential for developing new optofluidic applications.

Keywords Periodic liquid-air structure, Hollow optical fiber, Microscopic heat source, Sub-picoliter, Band-rejection filter

The Plateau–Rayleigh instability, frequently referred to simply as Rayleigh instability, constitutes a fundamental principle in physics and fluid mechanics, delineating the conditions under which a fluid column will disintegrate into distinct droplets[1,2]. This phenomenon is primarily driven by the propensity of surface tension to curtail the fluid's surface area, leading to spherical droplets forming in free space.

An alternate significant physical mechanism for the formation of liquid droplets involves liquid boiling within a confined space[3,4]. When a liquid traverses a narrow channel under specific heating conditions, the cyclical vaporization and condensation process dictates the distribution of liquid droplets in space. This method has been the subject of extensive research, particularly in the context of micro-cooling systems for electronic devices[5].

The formation of ultra-small fluidic droplet structures, in particular, has garnered considerable attention within the field of nano-microfluidics. This can be attributed to the fact that droplets can serve pivotal roles in a broad range of interdisciplinary applications. Ultra-small droplets can be used in drug delivery systems, where precise doses of medication are encapsulated in droplets and then delivered to targeted locations in the body[6,7]. They can also serve as miniaturized reaction vessels where chemical or biological reactions occur[8,9]. In producing advanced materials, small droplets can be used as templates for creating complex structures with unique properties[10,11]. Creating ultra-small droplets is fundamental to inkjet printing technology, where tiny droplets of ink are precisely deposited onto a substrate[12,13]. Understanding the properties and behavior of ultra-small droplets is also critical for modeling cloud formation and predicting weather and climate patterns[14].

Generating ultra-small droplets with controlled characteristics is pivotal across various interdisciplinary scientific and technological domains. Numerous methodologies have been employed to achieve this, including the use of piezoelectric actuators[15,16], T-junction formation[17], and co-planar electrodes[18]. Each technique presents distinct advantages and limitations. The piezoelectric actuator-based approach capitalizes on the mechanical strain induced by electric fields to achieve precise droplet formation. Conversely, the T-junction

[1]Institute of Physics and Applied Physics, Yonsei University, 50 Yonsei-ro, Seodaemun-gu, Seoul 03722, Republic of Korea. [2]LG Electronics, 222 LG-ro, Jinwi-myeon, Pyeongtaek-si 17709, Gyeonggi-do, Republic of Korea. [3]LG Display, 245, LG-ro, Wollong-myeon, Paju-si, Gyeonggi-do, Republic of Korea. [4]Optoelectronic Research Center, University of Southampton, SO17 1BJ Highfield, Southampton, UK. [5]Samsung Display, 1 Samsung-ro, Giheung-gu, 17113 Yongin-si, Gyeonggi-do, Republic of Korea. ✉email: koh@yonsei.ac.kr

method, characterized by a T-shaped intersection within the microfluidic channel, regulates flow rates to facilitate the production of droplets and periodic droplet structures within the microchannels[19,20]. Furthermore, the co-planar electrode technique utilizes electric fields to dictate droplet size and frequency, underscoring its utility in precise droplet manipulation.

While these methodologies have demonstrated efficacy in producing ultra-small droplets, they are not devoid of challenges. The chief limitations reside in the requisite system size and the process complexity. The relatively large scale of the necessary apparatus for these methods, particularly in the case of the electrically driven platforms, can often impose limitations on their practical deployment for in-situ droplet processing. Moreover, the intricate processes involved, such as the meticulous control of the electrical field or flow rates, further compound the operational difficulty. Therefore, while these techniques have significantly advanced the field of droplet microfluidics, there is a persistent need for novel approaches that can surmount these challenges. Further research is warranted to develop more compact and less complex methods for consistently generating ultra-small droplets and expanding to photonic applications. Recent advancements in fiber optic optofluidics have significantly enhanced the integration of optical fibers with microfluidic systems, offering new possibilities for highly sensitive and real-time detection of chemical and biological analytes. Researchers have developed innovative fiber-based optofluidic devices, particularly for lab-on-a-chip applications, which are proving useful in areas such as medical diagnostics and environmental monitoring[21]. Additionally, advances in fabrication techniques and materials, along with the exploration of novel fiber structures[22], have further improved the precision and efficiency of these systems. The author's research group reported the creation of a self-assembled periodic structure made of solid polymer and air inside a hollow optical fiber (HOF)[23]. The process involved two straightforward steps: first, filling the HOF with liquid polymer, and second, curing the polymer by irradiating UV light from the outside. These simple steps resulted in highly consistent and reproducible outcomes, particularly in terms of the period and duty cycles of the structure. The main mechanism behind this success was attributed to a combination of self-assembly, which conformed to the HOF's inner surface, and the liquid-to-solid phase transition. However, controlling the volume of the individual solid polymer elements within the periodic structure was not flexible. The viscosity of the liquid polymer and the chemistry of the curing process were identified as key parameters to increase the process's flexibility.

In the present study, we experimentally demonstrated a self-assembled, periodic, ultra-small fluidic structure synthesized by navigating a microscopic heat source (MHS) along a liquid-filled HOF. The overall schematics of this study are shown in Fig. 1. Figure 1(a) depicts a segment of HOF continuously filled with a low-viscosity liquid, whose ends were fusion-spliced with single-mode fibers (SMFs). When the HOF was heated using a tapering process in an advanced fusion splicer, its hole collapsed, forming a solid core that matched the mode field diameter of SMF[24]. The overall splice loss in SMF-HOF-SMF structure was ~1.0 dB, consistent with the findings reported in Ref. [24]. The HOF, featuring a central air hole, a germanosilica ring core, and a silica cladding in the inset of Fig. 1(a)[24,25], can uptake liquid via capillary action. As shown in the upper diagram of

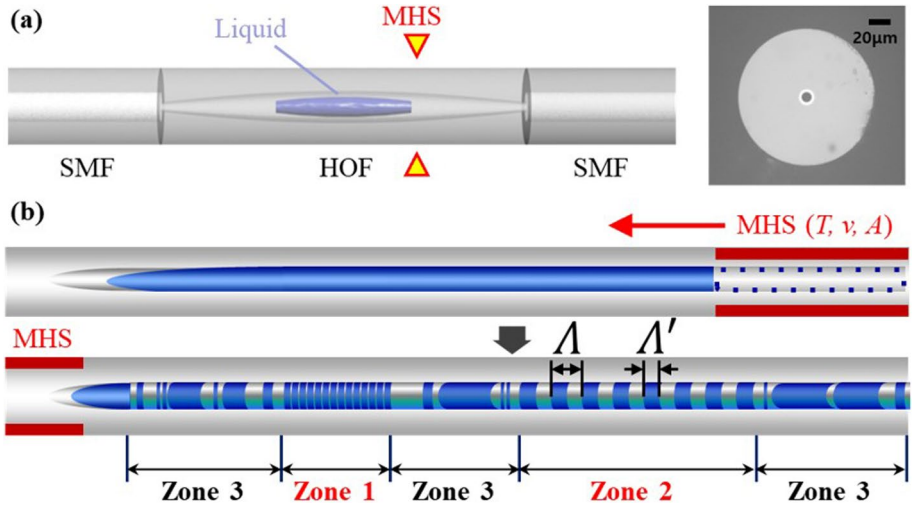

Figure 1. Schematic diagram for the formation of distinctive zones composed of liquid droplet-air structure inside a hollow optical fiber (HOF). This structure was obtained by single one-way traversing of a microscopic hot source (MHS) along the axial direction of HOF. (**a**) Experimental set-up to generate a periodic liquid droplet-air structure. A segment of liquid-filled HOF was spliced at both ends with single mode fibers (SMFs). The right inset shows a cross-section of HOF, which shows the central air hole, the light-guiding ring core, and the silica cladding. The bright ring represents the ring core. (**b**) Liquid structure inside HOF before the MHS traverse (above) and after a one-way MHS traverse (below). MHS was mounted on a stage whose movement can be electronically varied. MHS parameters were temperature (T), traverse velocity (v), and heating area (A). Zone 1 has a constant period of liquid droplet-air structure, Zone 2 has a variable period, and Zone 3 shows chaotic behavior. Λ is the period of liquid droplet-ai structure in Zone 1 and Zone 2. Λ′ is the thickness of the liquid droplet.

Fig. 1(b), we traversed MHS axially along the liquid-filled HOF using a commercially available motorized stage. The proposed fabrication process was controlled by straight forward parameters of the MHS-zone temperature (T), its traverse speed (v), and heating area (A) for a given set of parameters for the HOF geometrical structure and the liquid with a specific boiling temperature. In experiments, we kept v, and A at optimal values while primarily adjusting T. Irregularities in the structural parameters of the HOF were negligible over the process length of less than 10 cm. We used commercially available high-purity liquids to minimize impurities, effectively eliminating any uncertainty in the liquid's boiling temperature. We used a commercial motorized linear translation stage to electronically control MHS traverse speed, $v \sim 5$ mm/sec, and it showed an error less than 0.1%. The traverse speed was kept constant during the experiments.

Two types of MHS were used in this study, a commercial micro-oxyhydrogen torch (MOT)[26] and a ring-type metal heater (RMH)[27]. MOT was held by a mechanical x-y-z positioner mounted on the translation stage to precisely control the flame size and its distance from the HOF, allowing us to maintain A at around 4 mm^2. In MOT, both T and A were affected by the flow rate of oxygen and hydrogen, which was controlled by mass flow controllers (MFCs) and pressure regulators. The usual error range of the flow in MFCs are known to be $1 \sim 5\%$ for a normal laboratory environment without tight temperature-humidity-dust control[28]. Subsequently T and A, showed variation comparable to the MFC error range, which can affect the reproducibility of the process.

In order to further improve the reproducibility, we employed an all-electrically controlled MHS, an RMH. We used RHM which is a part of the Vytran glass processor-VGP[27]. The heating was tightly confined in an open-cut hollow circular slot with a diameter of 300 mm, where we inserted HOF, fixing $A \sim 3$ mm^2. We estimated the uncertainties: ± 1 °C in T in the RMH and the heating area was defined by the heater's geometry, with an estimated uncertainty of less than 0.5% in A. An electronically controlled RMH could provide a higher level of reproducibility but fundamental control of environment such as room temperature, humidity, and dust level could be practical issues as well.

Even with this simple configuration, we procured a periodic structure comprising alternating sequences of liquid droplets and air inside HOF. The characteristics of these liquid-air structures were subjected to comprehensive experimental analyses, which revealed three distinctive zones. They are schematically shown in the lower part of Fig. 1(b). Zone 1 exhibited near-constant periodicity regardless of changing process parameters. Conversely, the second zone, termed Zone 2, uniquely allowed adaptability in its periodicity, allowing for flexible control of both the period (Λ) and the thickness (Λ') of liquid droplets. In the third and final zone, Zone 3, the response was found to be chaotic with respect to MHS parameters. The origin of Zone 3 is not being fully understood at present, but we noted that its location was consistently near the SMF-HOF splice. In fiber preparation, we tried to maintain the adiabatic mode transformation along SMF to HOF or vice versa[24] to minimize the overall splice loss. The hole diameter of HOF monotonically decreased and collapsed to form a solid core at the SMF interface by using the tapering process in the splicer[27]. We observed that Zone 3 occurred near this tapering zone, and we speculate that the pressure buildup in the tapered hole led to the formation of a non-periodic structures. If we use a significantly longer length of the liquid filled segment in HOF to avoid the tapering splice region in the process, we could potentially reduce the size of Zone 3. However, since the liquid was introduced into the HOF through capillary action, the length of the HOF filled with liquid was limited. An effort to increase the liquid-filled length in a longer HOF by external means is being pursued by the authors. Further refining the process parameters for Zone 2, we obtained sub-picoliter liquid droplets separated by air within a HOF for the first time, to the author's best knowledge. In the following sections, we delineate the exgperimental conditions under which the liquid droplet-air structure in HOF was studied, as well as our observations pertaining to their characterization.

Results

Firstly, we fusion spliced one facet of HOF with a cleaved SMF, leaving the other facet of HOF open. We structured the one side closed channel with HOF and SMF. Then, we filled the HOF with deionized (DI) water by the capillary force. According to Washburn's equation[29], the length of the liquid-filled segment (L) by the capillary force is given by

$$L^2 = \left(\frac{\gamma}{\eta}\frac{cos\theta}{2}\right) rt, \tag{1}$$

where θ is the contact angle and t is the time for a liquid of viscosity η, and surface tension γ to a distance L into a capillary of radius r. In our experiments, we used a HOF with a hole diameter of 6.3 μm, L was approximately 1.8 cm for DI water and $t \sim 1.0$ s, which was consistent with the estimation given by Eq. (1).

After filling the HOF with water, the open-facet of HOF was fusion spliced to another SMF, as schematically shown in Fig. 1(a). A microscopic heat source (MHS) created a hot zone, and it brushed the DI water-filled HOF in the axial direction. We used two types of MHS: a C-type MOT, whose temperature was controlled by the flow rates of propane gas and O_2, and a RMH, whose temperature was controlled by the input electric power. MHS was mounted on a motorized stage, and we traversed the MHS along the axial direction of HOF. MHS parameters were temperature (T), traverse velocity (v), and heating area (A) over the HOF. T was varied in the range of $100 \sim 200$ °C, which was measured near the outside surface of HOF using a thermocouple. v was maintained at ~ 1 mm/sec. The C-type MOT provides two hot spots, top and bottom, and each spot has a heating area of $A \sim 4$ mm^2. The RMH provided a uniform ring hot zone over the whole circumference of HOF, whose thickness was $1 \sim 2$ mm. Here, we took only one unidirectional traverse of MHS. Due to the chaotic behavior of Zone 3 in Fig. 1(b), our systematic discussions focus only on Zone 1 and 2 in the following sections. Note that when we varied T, we repeated the experiments with new samples to take consistent measurements.

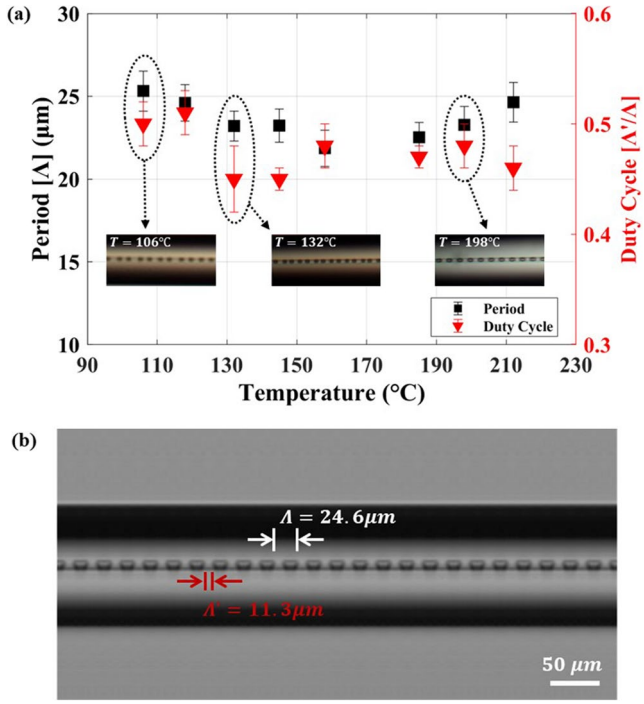

Figure 2. Zone 1 formed using a C-type oxyhydrogen torch MHS. (**a**) Variations in Λ and DC in Zone 1 as a function of MHS temperature. The insets are images taken from a fusion splicer at the given temperatures. In the center of HOF, water segments are shown bright, and dark regions represent the air segments. (**b**) High-resolution optical microscope images of Zone 1 at T = 212 °C. (MHS: micro heating source, Λ: average period of the water-air structure, Λ': average thickness of the water segment. DC: Duty Cycle).

T (℃)	Λ (μm)	Λ' (μm)	Λ'/Λ
106	25.3	12.7	0.50
118	24.6	12.6	0.51
132	23.2	10.4	0.45
145	23.2	10.5	0.45
158	21.9	10.5	0.48
185	22.5	10.6	0.47
198	23.3	11.2	0.48
212	24.6	11.3 5	0.46

Table 1. Air-water droplet period, droplet thickness, and duty cycle in Zone 1 for various temperatures. Here, the values are the average of each measurement.

As the MHS completed its unidirectional single transverse over the water-filled HOF, self-assembled water-air structures formed along the axial direction, as shown schematically in the bottom of Fig. 1(b). In Zone 1, the water-air periodic structure inside the hole displayed a well-defined liquid droplet-air period (Λ) and a liquid droplet thickness (Λ'), both of which were nearly temperature-independent. The length of Zone 1 ranged from 400 to 500 μm.

Within the temperature range of 106 to 212 °C, we captured microscopic images from a fusion splicer over Zone 1, some of which are shown in the inset of Fig. 2(a). Our periodic structures have pitches around 20 μm and droplet thicknesses of about 10 μm, as summarized in Table 1. To optically analyze these structures, we need a laser wavelength (λ) that matches the structure pitch (Λ)[30], which corresponds to a CO_2 laser. However, CO_2 lasers are strongly absorbed by both the silica cladding of the HOF and the water in the core, leaving little to no interferometric information. Additionally, the cylindrical surface of the HOF causes collimated incident light to focus, only to rapidly defocus upon exiting, resulting in secondary or even tertiary interference, which makes the analysis much more complex.

To address this, we used an advanced fiber optic fusion splicer, which has a feature that allows us to manually adjust the focus. This can either be aligned with the cladding surface for cladding splicing or centered on the core for core-aligned splicing[31]. By continuously controlling the focal point, we were able to capture optimal images for our experiments. In Fig. 2(a), average values of and the duty cycle (DC), Λ'/Λ, are plotted as a function of

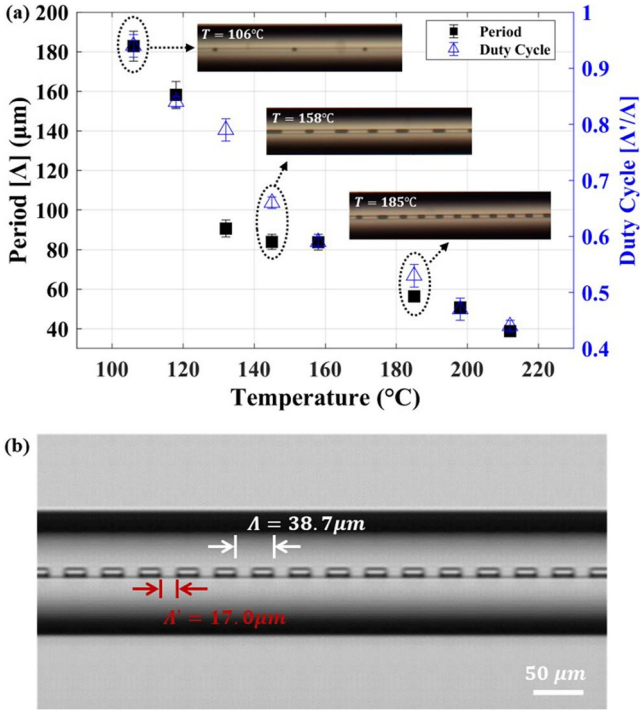

Figure 3. Zone 2 formed using a C-type oxyhydrogen torch MHS. (**a**) Variations in Λ and DC in Zone 2 as a function of MHS temperature. The insets are images taken from a fusion splicer at the given temperatures. In the center of HOF, water segments are shown bright, and dark regions represent the air segments. (**b**) High-resolution optical microscope images of Zone 2 at MHS temperatures T = 212 °C. (MHS: micro heating source, Λ: average period of the water-air structure, Λ': the average thickness of the water segment.).

T (℃)	Λ (μm)	Λ' (μm)	Λ'/Λ
106	182.8	171.8	0.94
118	158.2	132.9	0.84
132	90.7	71.6	0.79
145	83.9	55.4	0.66
158	83.8	49.4	0.59
185	56.3	29.9	0.53
198	50.7	23.8	0.47
212	38.7	17.0	0.44

Table 2. Air-water droplet period, droplet thickness, and duty cycle in Zone 2 for various temperatures. Here, the values are the average of each measurement.

MHS temperature (T). The variation remained narrow to 22 to 25 μm, and DC was between 0.45 and 0.50. This periodic structure was surprisingly regular despite the MHS temperature doubling. Figure 2(b) shows a high-resolution optical microscopic image of Zone 1 at T = 212 °C, with a clear distinction between water segments and air.

In Zone 2, we observed periodic water-air structures where both Λ and Λ' consistently changed with T. The length of Zone 2 was similar to that of Zone 1. We captured microscopic images from a fusion splicer over Zone 2, and some of these images are shown in the inset of Fig. 3(a). More detailed measurement results are summarized in Table 2. In Fig. 3(a), the average values of Λ and DC are plotted against T. As T increased, both of them decreased monotonically. The Λ decreased from 182.8 to 38.7 μm, which is about a five-fold reduction in the temperature range of 106 to 212 °C. DC decreased from 0.94 to 0.44, more than halving over the same temperature range. Notably, larger water droplets formed at the lower temperature range of about 100 to 130 °C, with a DC of 0.85 to 0.93. In this lower temperature range, the air segment length was significantly short, about one-tenth to one-ninth of the water droplet length. As T increased beyond 180 °C, the air segment length increased significantly, dropping the DC to 0.5 or less. Another noteworthy observation is that the periodic structures of Zone 1 and Zone 2 started to converge as T exceeded 180 °C. In Fig. 3(b), a high-resolution optical microscopic image of Zone 2 at T = 212 °C shows the regularity of the periodic water-air structure. The similarity

between Fig. 2(b) and Fig. 3(b) confirms the convergence of the periodic structures in Zones 1 and 2 at higher temperatures.

For the measurements in Zone 2, we further estimated the volume of individual water droplets. Here, we approximated the water droplet as a circular plate whose diameter is the same as the hole diameter (D) of HOF, and its height is the average Λ' of the given periodic structure to have the volume of $V_{droplet} = \pi\,(D/2)^2\Lambda'$. Figure 4(a) illustrates the variation in the water droplet volume of water droplets within Zone 2 in response to MHS temperatures. It is noted that the water droplet volume monotonically decreased with increasing temperature. It is assumed that the liquid droplet broke into smaller volumes at a high temperature to accommodate the relative temperature difference between the preceding MHS and the cooled HOF segment following behind. Drawing upon the preceding findings, we demonstrate the capability to generate liquid droplets spanning from hundreds of femtoliters to a few picoliters in volume within the periodic structure in HOF.

In Fig. 4(b)~(c), we further investigate how the periodic structures changed with types of liquids. We chose isopropyl alcohol and ethanol such that their boiling temperatures T^B satisfied T^B_{water} (100℃) > $T^B_{isopropyl\ alcohol}$ (82.3℃) > $T^B_{ethanol}$ (78.4℃). For the lower boiling temperature liquids, we observed a notable increase in the air segment length $\Lambda' = 29.7\ \mu$m in Fig. 4(b) and $\Lambda' = 5.8\ \mu$m in Fig. 4(c). These changes subsequently reduced DC = 0.18 in Fig. 4(b) and DC = 0.08 in Fig. 4(c), which were not observable in water cases in Fig. 2, and Fig. 3. It is observed that the low T^B liquid provided larger air segments to reduce DC. which is related to boiling and recondensation process for the liquid in the experiments. These observations showed a high potential to flexibly vary the liquid-air periodic structures by proper choices of liquid's physical characteristics, which is being further pursued by the authors.

To assess the optical properties of water-filled HOF, we conducted transmission measurements using a white light source (Yokogawa AQ4305) and an optical spectrum analyzer (Agilent 86142 A). In Fig. 5(a), a pristine HOF exhibits the LP11 mode cut-off wavelength, λ_{cutoff} ~ 1290 nm before the water filling. When the water was filled, λ_{cutoff} shifted toward a shorter wavelength near 850 nm. In a step-index fiber with the core refractive index n_1, cladding index n_2, and the core diameter D, λ_{cutoff} is defined as below[32].

$$\lambda_{cutoff} = \frac{\pi D\sqrt{n_1^2 - n_2^2}}{2.405} \tag{2}$$

HOF has a ring core with two asymmetric interfaces: the inner interface with the air at the central hole and the silica cladding. When the water replaces the air in the central hole, the difference in the refractive index between the ring core and the central hole significantly decreases to shift λ_{cutoff} to a shorter wavelength.

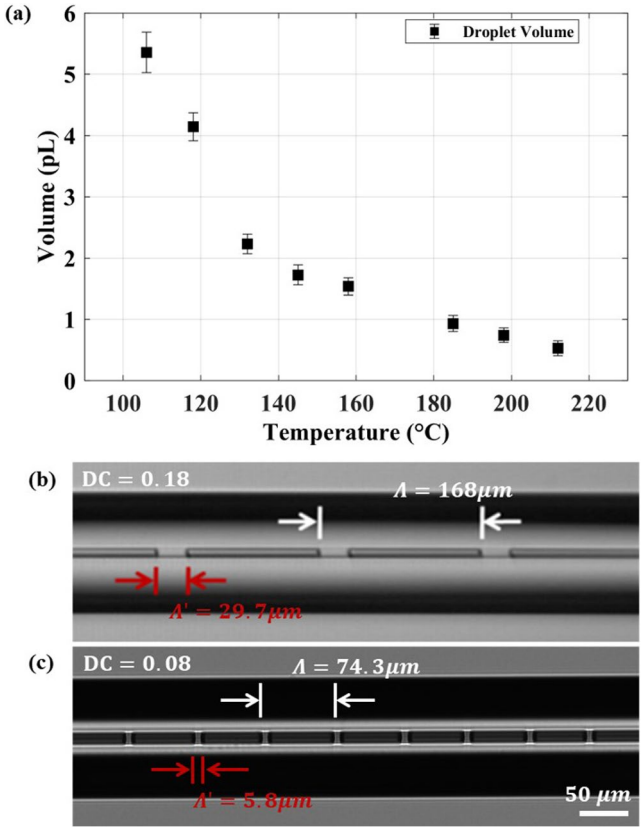

Figure 4. (**a**) Volume of the water droplet with temperature varying from 212 °C to 106 °C in Zone 2. (**b**) Isopropyl alcohol (**c**) Ethanol.

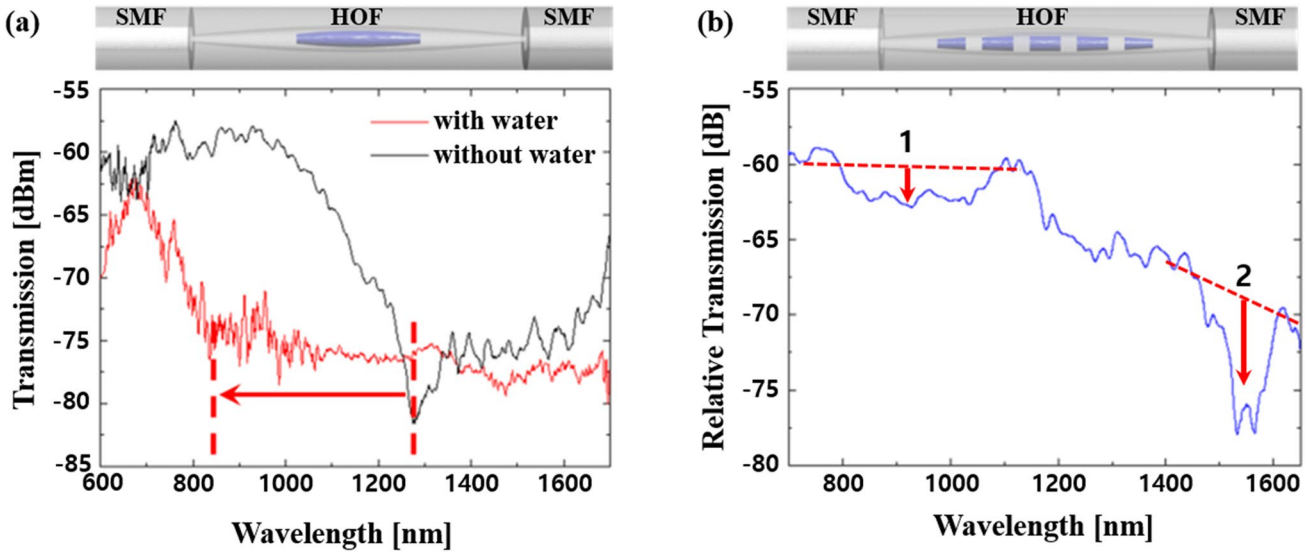

Figure 5. (**a**) Comparison of transmission spectra of HOF with water and without water. The water-filled HOF segment length was ~2 cm. (**b**) Relative transmission for a water-air periodic structure. Here, we subtracted the transmission of HOF with the water-air periodic structure from that of HOF filled with water. Two band rejection filter characteristics are indicated by arrows 1 and 2.

After making a water-air periodic structure, we measured the transmission spectrum and subtracted it from that of HOF filled with water. Here, the structure had all Zone 1, Zone 2, and Zone 3. It was prepared at T = 212 °C so that the periodic structures in Zone 1 and Zone 2 converged to each other. The results are shown in Fig. 5(b). We observed two band-rejection filter characteristics, as shown in arrows 1 and 2. Band-1 has a broad bandwidth of ~150 nm with a maximum rejection efficiency of 2.5 dB, while band-2 has a full-width half maximum (FWHM) of ~30 nm and a maximum rejection of ~6 dB. The ring core surrounds the air-water periodic structure, and the periodic arrangement modulates the refractive index to form a long-period grating (LPG)[33]. The phase matching condition between the core guided LP^{core}_{01} mode and the cladding modes LP^{clad}_{lm} is given below for a grating period of Λ_{grating}.

$$\beta_{01}^{core} - \beta_{lm}^{clad} = \frac{2\pi}{\Lambda_{grating}} \tag{3}$$

In conventional UV-induced LPGs, Λ_{grating} is typically between $200 \sim 500 \mu m$ and the index modulation $\Delta n \sim 10^{-4}$ to 10^{-3}, to have band rejection of 10 ~ 25 dB in the optical communication window near 1550 nm. Note that in HOF, the light is guided in the ring core, and the periodic water-air droplet can provide a refractive index modulation. However, the refractive index modulation Δn was not estimated since the net interaction between the light in the ring core and the water segments was not fully understood yet. Compared to conventional UV-induced LPGs, our water-air structure in HOF has a fraction of periodicity, where its high harmonics may satisfy the phase-matching condition with a lower band rejection efficiency. In further studies to characterize the band-rejection characteristics of the proposed device, it might be necessary to include multimode interference effects[34] among the cladding modes of HOF[35] excited at SMF-HOF splices. Non-ideal adiabatic mode transformation at SMF-HOF splices can excite cladding modes, which can interfere with one another to make the output transmission spectrum much more complex than the ideal phase-matching cases. The authors are pursuing the investigation of these band rejection characteristics to clarify their origin.

Furthermore, we have Zones 1, 2, and 3 in the prepared HOF, and non-uniform periodicity variations could affect the mode-coupling to reduce the band rejection efficiency. Even though the performance as a band rejection filter was not comparable to prior UV-induced LPGs, our experiments showed a potential to use the liquid-air periodic structure in optical applications. Notably, the liquid-air structure maintained its periodicity under vibration but showed a significantly high response to temperature changes (10 ~ 80 °C, a clinically important temperature range) and bending. Despite its liquid nature, the proposed structure showed significant resilience against external physical perturbations, such as temperature, humidity, and vibrations. It is noteworthy that the liquid structures were embedded inside HOF, which is made of silica. The outer diameter of HOF silica cladding was ~125 mm, while the central hole, where periodic liquid structures were present, had diameter of ~6 mm. This large ratio in both surface area and the volume imply that the responses to external thermo-mechanical perturbations would be mainly determined by the silica cladding. We have not observed any significant variations of the periodic structures during the experiments and after several days in the lab environment. While ambient temperature fluctuations potentially induce the instability through thermal expansion or contraction of both the HOF and the liquid droplets[36,37], conventional electronic temperature control with a suitable packaging can minimize such effects.

In this report, we used liquids without specific optical functionalities. By incorporating optically functional materials into the liquid, the proposed structure could have unique photonic applications. For example, dissolving an optical dye or quantum dots in a high refractive-index liquid could create an array of optical gain media, coupled through the circular ring core of the HOF. Each droplet could act as a micro-optical liquid cavity[38], with lasing characteristics mainly governed by whispering gallery modes[39]. This structure offers a novel way to explore the laser dynamics of serially coupled laser cavities, pumped by the HOF's ring core. Compared to solid grating structures embedded in optical fibers, the periodic liquid droplets in our design could be more sensitive to external factors like temperature, strain, and acceleration, opening up new possibilities for optical sensing applications. The authors are pursuing further sensor applications of the proposed liquid-air structure in HOF.

Conclusion

In this study, we conducted experiments to demonstrate the formation of self-assembled, periodic, liquid droplet-air structures within a hollow optical fiber (HOF) by maneuvering a micro heat source (MHS) along a liquid-filled HOF. The experimental process involved filling the HOF with a low-viscosity liquid, such as DI water, isopropyl alcohol, or ethanol, followed by fusion splicing both ends with single mode fiber (SMF). As the MHS traversed with a temperature range of 100 °C to 210 °C, alternating sequences of liquid droplets and air within the HOF were formed. These structures were categorized into three distinct zones. Zone 1 exhibited near-constant periodicity with Λ ranging from 21.9 to 25.3 µm and duty cycle (DC) between 0.45 and 0.50, regardless of the MHS temperature. In contrast, Zone 2 displayed variable structure with both Λ and DC decreasing monotonically as the temperature increased, ranging from 182.8 to 38.7 µm and 0.94 to 0.44, respectively. Zone 3 demonstrated chaotic behavior, rendering it less suitable for controlled applications. Furthermore, we investigated the influence of using different liquids, such as isopropyl alcohol and ethanol, on the periodic structures. Lower boiling point liquids resulted in increased air segment lengths and decreased duty cycles, indicating the possibility of tailoring the liquid-air periodic structures by selecting appropriate liquids. We further examined the optical properties of the water-filled HOF. Transmission measurements revealed that while a pristine HOF had an LP_{11} mode λ_{cutoff} of approximately 1290 nm, filling it with water shifted λ_{cutoff} to around 850 nm. Further analysis of a water-air periodic structure prepared at 212 °C unveiled two band-rejection filter characteristics: Band-1 with a broad bandwidth of ~ 150 nm and a maximum rejection efficiency of 2.5 dB, and Band-2 with a FWHM of ~ 30 nm and a maximum rejection of ~ 6 dB. Future research endeavors may explore utilizing these periodic fluidic structures for optical sensing and filtering applications, as well as for developing novel optical devices with tailored properties.

Data availability

The datasets generated during and/or analyzed during the current study are available from the corresponding author on reasonable request.

Received: 3 June 2024; Accepted: 9 October 2024
Published online: 31 October 2024

References

1. Kundu, P. K., Cohen, I. M. & Dowling, D. R. *Fluid mechanics*. (Academic press, 2015).
2. Mead-Hunter, R., King, A. J. & Mullins, B. J. Plateau Rayleigh instability simulation. *Langmuir* **28**, 6731–6735 (2012).
3. Lin, S., Sefiane, K. & Christy, J. Prospects of confined flow boiling in thermal management of microsystems. *Appl. Therm. Eng.* **22**, 825–837 (2002).
4. Zhang, G., Liu, Z. & Wang, C. A visualization study of the influences of liquid levels on boiling and condensation co-existing phase change heat transfer phenomenon in small confined spaces. *Int. J. Heat Mass Transfer* **73**, 415–423 (2014).
5. Hetsroni, G., Mosyak, A., Pogrebnyak, E. & Segal, Z. Explosive boiling of water in parallel micro-channels. *Int. J. Multiphase Flow* **31**, 371–392 (2005).
6. Riahi, R. et al. Microfluidics for advanced drug delivery systems. *Curr. Opin. Chem. Eng.* **7**, 101–112 (2015).
7. He, F. et al. Designable polymeric microparticles from droplet microfluidics for controlled drug release. *Adv. Mater. Technol.* **4**, 1800687 (2019).
8. Totlani, K., Hurkmans, J.-W., Van Gulik, W. M., Kreutzer, M. T. & Van Steijn, V. Scalable microfluidic droplet on-demand generator for non-steady operation of droplet-based assays. *Lab. Chip* **20**, 1398–1409 (2020).
9. Zeng, Y. et al. Miniaturizing chemistry and biology using droplets in open systems. *Nat. Rev. Chem.* **7**, 439–455 (2023).
10. Song, Y., Hormes, J. & Kumar, C. S. Microfluidic synthesis of nanomaterials. *Small* **4**, 698–711 (2008).
11. Bae, J., Lee, J., Zhou, Q. & Kim, T. Micro-/nanofluidics for liquid-mediated patterning of hybrid-scale material structures. *Adv. Mater.* **31**, 1804953 (2019).
12. Guo, Y., Patanwala, H. S., Bognet, B. & Ma, A. W. Inkjet and inkjet-based 3D printing: connecting fluid properties and printing performance. *Rapid Prototyping J.* **23**, 562–576 (2017).
13. Wijshoff, H. Drop dynamics in the inkjet printing process. *Curr. Opin. Coll. Interf. Sci.* **36**, 20–27 (2018).
14. Haywood, J. in *Climate change* 645–659 (Elsevier, 2021).
15. Bransky, A., Korin, N., Khoury, M. & Levenberg, S. A microfluidic droplet generator based on a piezoelectric actuator. *Lab. Chip* **9**, 516–520 (2009).
16. Lu, S., Zhang, J., Liu, Y., Zheng, H. & Ren, C. Droplet formation study of a liquid micro-dispenser driven by a piezoelectric actuator. *Smart Mater. Struct.* **28**, 055003 (2019).
17. Wu, H.-W., Huang, Y.-C., Wu, C.-L. & Lee, G.-B. Exploitation of a microfluidic device capable of generating size-tunable droplets for gene delivery. *Microfluid. Nanofluid.* **7**, 45–56 (2009).
18. Ahmed, R. & Jones, T. Dispensing picoliter droplets on substrates using dielectrophoresis. *J. Electrost.* **64**, 543–549 (2006).
19. Chin, L., Liu, A., Zhang, J., Lim, C. & Soh, Y. An on-chip liquid tunable grating using multiphase droplet microfluidics. *Appl. Phys. Lett.* **93**, 16 (2008).
20. Shen, Z., Zou, Y. & Chen, X. An integrated microfluidic signal generator using multiphase droplet grating. *Microfluid. Nanofluid.* **14**, 809–815 (2013).

21. Li, L. et al. Optical fiber optofluidic bio-chemical sensors: a review. *Laser Photon. Rev.* **15**, 2000526 (2021).
22. Shao, L., Liu, Z., Hu, J., Gunawardena, D. & Tam, H.-Y. Optofluidics in microstructured optical fibers. *Micromachines* **9**, 145 (2018).
23. Jung, H. et al. Mask-free hybrid long-period fiber grating fabrication by self-assembled periodic polymerization in silica hollow optical fiber. *Optics Lett.* **34**, 2745–2747 (2009).
24. Oh, K., Choi, S., Jung, Y. & Lee, J. W. Novel hollow optical fibers and their applications in photonic devices for optical communications. *J. Lightwave Technol.* **23**, 524–532 (2005).
25. Choi, S. & Oh, K. A new LP02 mode dispersion compensation scheme based on mode converter using hollow optical fiber. *Optics Commun.* **221**, 307–312 (2003).
26. HAMPDON. *Smith Style Little Micro Torch Kit with Regulators to Suit LPG / Oxygen*, <https://www.hampdon.com.au/smith-style-little-micro-torch-kit-with-regulators> (2024).
27. THORLABS. *Fiber Holder Bottom Inserts - Two Required for Single Fiber Processing*, <https://www.thorlabs.com/newgrouppage9.cfm?objectgroup_id=9326&pn=VHE20> (2024).
28. Giovino, B. *How to Accurately Monitor and Control Gas Flow in Industrial Applications*, <https://www.digikey.kr/en/articles/how-to-accurately-monitor-and-control-gas-flow-in-industrial-applications> (2022).
29. Washburn, E. W. The dynamics of capillary flow. *Phys. Rev.* **17**, 273 (1921).
30. Born, M. & Wolf, E. *Principles of optics: electromagnetic theory of propagation, interference and diffraction of light*. (Elsevier, 2013).
31. THORLABS. *Vytran® Automated Glass Processors*, <https://www.thorlabs.com/newgrouppage9.cfm?objectgroup_id=9355> (2024).
32. Oh, K. & Paek, U.-C. *Silica optical fiber technology for devices and components: design, fabrication, and international standards*. (John Wiley & Sons, 2012).
33. Vengsarkar, A. M. et al. Long-period fiber gratings as band-rejection filters. *J. Lightwave Technol.* **14**, 58–65 (1996).
34. Wang, K. et al. Advances in optical fiber sensors based on multimode interference (MMI): a review. *IEEE Sens. J.* **21**, 132–142 (2020).
35. Lee, S., Park, J., Jeong, Y., Jung, H. & Oh, K. Guided wave analysis of hollow optical fiber for mode-coupling device applications. *J. Lightwave Technol.* **27**, 4919–4926 (2009).
36. Xue, S., Barton, G. W., Fleming, S. & Argyros, A. Analysis of capillary instability in metamaterials fabrication using fiber drawing technology. *J. Lightwave Technol.* **35**, 2167–2174 (2017).
37. Deng, D., Nave, J.-C., Liang, X., Johnson, S. & Fink, Y. Exploration of in-fiber nanostructures from capillary instability. *Opt. Express* **19**, 16273–16290 (2011).
38. Giorgini, A., Avino, S., Malara, P., De Natale, P. & Gagliardi, G. Liquid droplet microresonators. *Sensors* **19**, 473 (2019).
39. Vollmer, F., Yu, D., Vollmer, F. & Yu, D. Whispering Gallery Modes in Optical Microcavities. *Optic. Whispering Gall. Modes Biosens.: Phys. Princ. Appl.*, 117–170 (2020).

Acknowledgements

This work was supported in part by the NRF under Grant ROA-2008-000-20054-0, Grant R15-2004-024-00000-0, and Grant 2008-8-1893 (the European Community's Seventh Framework Programme [FP7/2007-2013] under Grant agreement n° 219299, Gospel), in part by the ITEP under Grant 2009-8-0809, in part by the Brain Korea 21 Project of the KRF, and in part by the Institute for Information & communications Technology Promotion(I-ITP) grant funded by the Korea government(MSIP) (No.2021-0-01561, Nanoscale Quantum Emitters Integrated by All-fiber Optofluidics).

Author contributions

S.A. conceived and designed the experiments and wrote the manuscript. S.J. revised the manuscript and figure. J.H., Y.J. and J.K. participated in the experiment. K.O. supervised the project and contributed to manuscript writing, revision, and figure arrangements. All authors reviewed the manuscript.

Declarations

Competing interests

The authors declare no competing interests.

Additional information

Correspondence and requests for materials should be addressed to K.O.

Reprints and permissions information is available at www.nature.com/reprints.

Publisher's note Springer Nature remains neutral with regard to jurisdictional claims in published maps and institutional affiliations.